

The structure of a separating turbulent boundary layer. Part 2. Higher-order turbulence results

By ROGER L. SIMPSON, Y.-T. CHEW† AND
B. G. SHIVAPRASAD

Southern Methodist University, Dallas, Texas 75275

(Received 19 August 1980 and in revised form 16 March 1981)

The velocity-probability-distribution flatness and skewness factors for u and v are reported for the separating turbulent boundary layer described by Simpson, Chew & Shivaprasad (1981). Downstream of separation the skewness factor for u is negative near the wall, whereas it is positive upstream of separation. The flatness factor for u downstream of separation differs from the upstream behaviour in that it has a local maximum of about 4 at the minimum mean velocity location in the backflow. Both upstream and downstream of separation the skewness factor for v has a profile shape and magnitudes that are approximately the mirror image or negative of the skewness factor for u . The flatness factor for v seems to be affected little by separation.

Examination of the momentum and turbulence-energy equations reveals that the effects of normal stresses are important in a separating boundary layer. Negligible turbulence-energy production occurs in the backflow. Turbulence-energy diffusion is increasingly significant as separation is approached and is the mechanism for supplying turbulence energy to the backflow.

The backflow appears to be controlled by the large-scale eddies in the outer region flow, which provides the mechanism for turbulence-energy diffusion. The backflow behaviour does not appear to be significantly dependent on the far downstream near-wall conditions when the thickness of the backflow region is small compared with the turbulent shear layer thickness.

1. Introduction

This paper deals with the more detailed turbulence structure measured for the separating turbulent boundary layer described by Simpson *et al.* (1981). In that paper mean velocities and Reynolds stresses were reported from hot-wire and laser anemometer measurements.

Simpson *et al.* (1981) conclude that those measurements support the conclusions of Simpson, Strickland & Barr (1977). Those measurements also revealed that the backflow mean-velocity profile scales on the maximum negative mean velocity U_N and its distance from the wall N . A law-of-the-wall velocity profile is not consistent with this correlation since both U_N and N increase with streamwise distance, while the law-of-the-wall length scale ν/U_τ varies inversely with the velocity scale U_τ .

In the backflow u' and v' are of the same order as $|U|$. Correlations of Reynolds

† Present address: Department of Mechanical and Production Engineering, University of Singapore.

shearing stress $-\overline{uv}/u'v'$ and $-\overline{uv}/(u'^2+v'^2)$ are very low in the backflow and are about 25% lower in the outer region of the separated flow than in the upstream attached flow. Simpson *et al.* (1981) also showed that the mixing length and eddy viscosity models are meaningless in the backflow. Normal stresses effects appear to account for the lower mixing length and eddy viscosity values observed in the outer region of the separated flow.

The skewness and flatness factors for u and v have not been previously reported in the literature and are presented here. The effect of separation on these factors is discussed. Measurements of the turbulence kinetic energy diffusion flux are also reported. Momentum and turbulence-energy balances for this flow are presented together with their implications as to the nature of the backflow. Spectra of the streamwise velocity fluctuation u are presented for the separated flow, which have also not been previously reported in the literature.

2. Experimental equipment

A description of the wind tunnel and hot-wire and laser anemometers is contained in Simpson *et al.* (1981). Additional instrumentation was used to obtain the results presented here. Electronic multipliers (Analog Devices AD533JH) were used to produce the turbulence quantities uv , u^2v and v^3 from hot-wire data. These multipliers were trimmed to within $\pm 1\%$ full-scale nonlinearity error. True integrating voltmeters, each consisting of a voltage-controlled oscillator and a digital counter, were used to obtain true time-averaged results.

The same velocity probability histograms of laser anemometer data that were used to obtain the U , V , $\overline{u^2}$, $\overline{v^2}$ and $-\overline{uv}$ results described by Simpson *et al.* (1981) were used to obtain $\overline{u^3}$, $\overline{v^3}$, $\overline{u^4}$ and $\overline{v^4}$ presented here. At the same time that the histograms were obtained spectra were measured in the separated flow zone with a signal data rate of about 400/s. A Princeton Applied Research Model 4512 Fast-Fourier-Transform Spectrum Analyzer was used to obtain u spectral distributions.

3. Experimental results

To investigate the effect of separation on higher-order structure functions, the third and fourth moments given by

$$\overline{u^n} = \int_{-\infty}^{+\infty} (\mathcal{U} - U)^n P(\mathcal{U}) d\mathcal{U} \quad (1)$$

with $n = 3, 4$ were calculated from each \mathcal{U} and \mathcal{V} anemometer velocity histogram $P(\mathcal{U})$ and $P(\mathcal{V})$. Simpson & Chew (1979) showed that the skewness factors, $S_u = \overline{(u^3)}/(\overline{u^2})^{3/2}$ and $S_v = \overline{(v^3)}/(\overline{v^2})^{3/2}$, and flatness factors, $F_u = \overline{(u^4)}/(\overline{u^2})^2$ and $F_v = \overline{(v^4)}/(\overline{v^2})^2$, were about ± 0.1 and ± 0.2 uncertain. Data obtained on different days were in close agreement, with the scatter being within these uncertainty levels.

For purposes of comparison and for obtaining the diffusion flux of turbulence-kinetic-energy, $\overline{u^2v}$ and $\overline{v^3}$, triple correlation data were obtained from the cross-wire anemometer. The main source of uncertainty in these measurements is the drift of the mean voltage level in the multipliers. This was kept to a minimum by adjusting

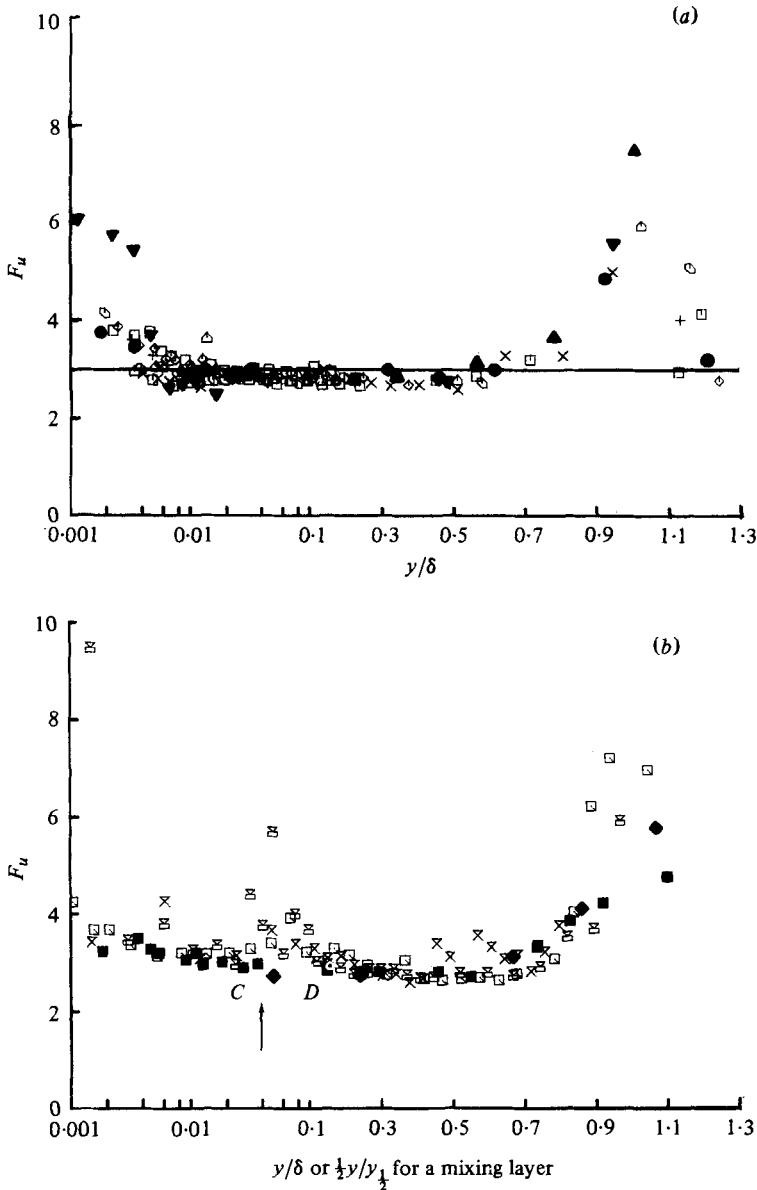


FIGURE 1. Flatness-factor, F_u , profiles (a) upstream and (b) downstream from separation. (a) \square , 112.4 in.; \square , 118.5; \triangle , 120.5; $+$, 122.6; \times , 127.1; \diamond , 129.4; \square , 131.9. Sandborn (1959): \bullet , near separation, $R_{\delta_2} = 5687$. Antonia (1973): \blacktriangle , $R_{\delta} = 31000$. Dumas & Marcellat (1966): $R_{\delta} = 32500$; —, value for Gaussian distribution. Note the log-linear abscissa. (b) C and D are the inflection points described by Shiloh *et al.* (1981) \blacksquare , 138.75 in.; \square , 144.9; \square , 156.4; \times , 170.9. The arrow denotes the location of minimum mean velocity U . \blacklozenge , Wygnanski & Fiedler (1970), mixing-layer data.

the offset voltage before, several times during, and after taking a set of data, so that a zero voltage input produced a zero voltage output. During data reduction a correction was applied for the offset voltage. All data which were greater than 25% uncertain are not presented here. This arbitrary uncertainty limit is not really very high, considering that third-order correlations are expected to have high uncertainties.

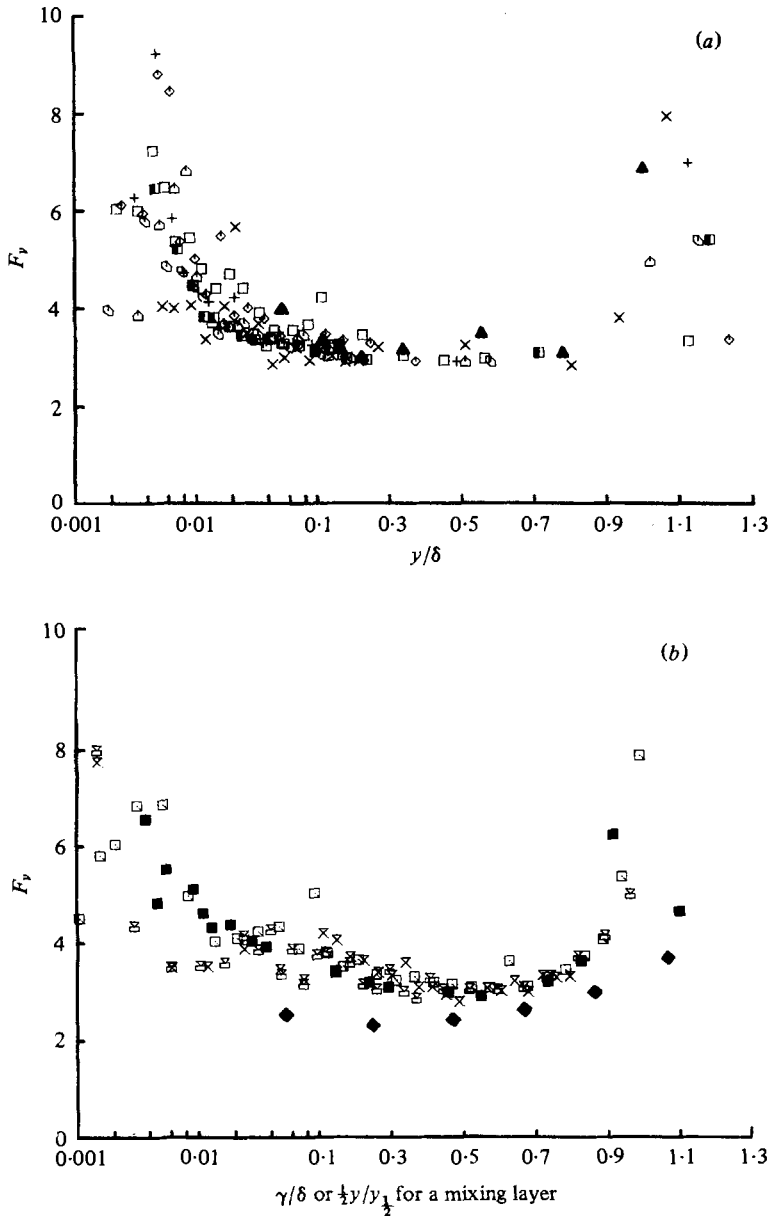


FIGURE 2. Flatness-factor, F_v , profiles (a) upstream and (b) downstream from detachment. (a) \blacksquare , 112.4 in.; \square , 118.5; \triangle , 120.5; +, 122.6; \times , 127.1; \diamond , 129.4; \square , 131.9. Antonia (1973); \blacktriangle , $R_\delta = 31\,000$. (b) \blacksquare , 138.75 in.; \boxtimes , 144.9; \square , 156.4; \times , 170.9. \blacklozenge , Wygnanski & Fiedler (1970), mixing-layer data. Note log-linear abscissa.

Simpson, Chew & Shivaprasad (1980) showed that the skewness factor S_v results obtained by laser and cross-wire anemometers for several streamwise locations are in agreement within the estimated uncertainties. In the separated zone the hot-wire measurements were confined to the outer region where the instantaneous flow direction differed less than 45° from the mean flow direction.

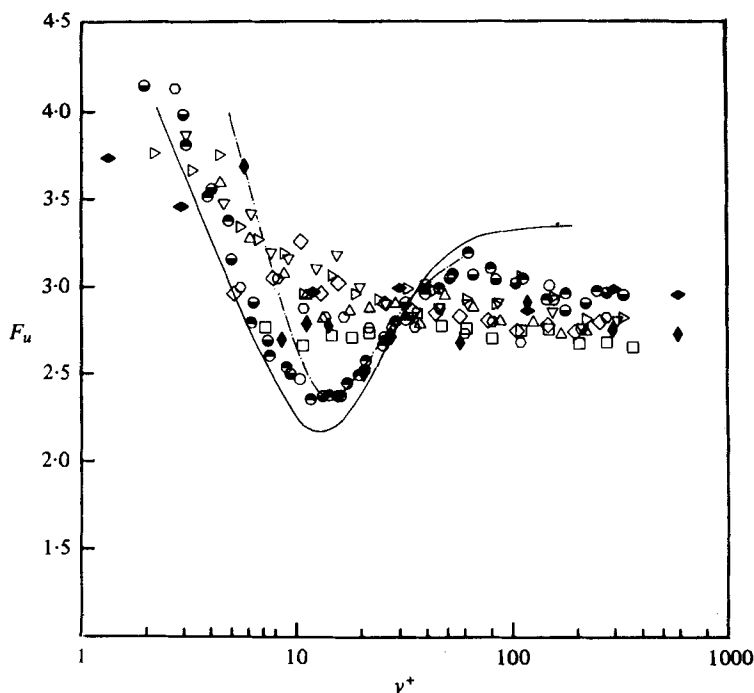


FIGURE 3. F_u versus y^+ upstream from detachment: \square , 112.4 in.; \circ , 118.5; \triangle , 122.6; \diamond , 120.5; ∇ , 129.4; \triangleright , 131.9. Ueda & Hinze (1975) \bullet , $Re = 35\,500$; \ominus , $Re = 11\,450$. \blacklozenge , Sandborn (1959); \blacklozenge , Dumas & Marcillat (1966); —, Kreplin (1973); - - -, Zaric (1972).

4. Discussion of higher-order correlations

4.1. Skewness and flatness-factor distributions

Some measurements of skewness and flatness factors of the u and v fluctuations have been done in zero-pressure-gradient boundary layers and in channel flows by Dumas & Marcillat (1966), Zaric (1972), Kreplin (1973), Antonia (1973) and Ueda & Hinze (1975). Only Sandborn (1959) is known to have made measurements of the flatness factor in an adverse-pressure-gradient boundary-layer flow in the vicinity of separation.

Figures 1(a) and 2(a) show a comparison of the present laser-anemometer data for F_u and F_v with the zero-pressure-gradient boundary-layer data of Antonia (1973). The close agreement observed between the two sets of data in the logarithmic region and the outer region indicates that the pressure gradient does not have much effect on F_u and F_v in those regions. Comparison with figures 1(b) and 2(b) for the flow downstream of separation also indicates that separation does not have much effect on F_u and F_v over the shear layer.

However, when plotted against y^+ in figure 3, the data for F_u upstream of separation indicate an apparent effect of pressure gradient in the region close to the wall, mainly in the buffer layer $8 < y^+ < 20$. In the viscous sublayer for both zero and adverse-pressure-gradient flows, the flatness factor attains values much higher than the value for a Gaussian probability distribution, which is equal to 3. This is possible because the inrush phase of the bursting cycle which brings in high-velocity fluid from the

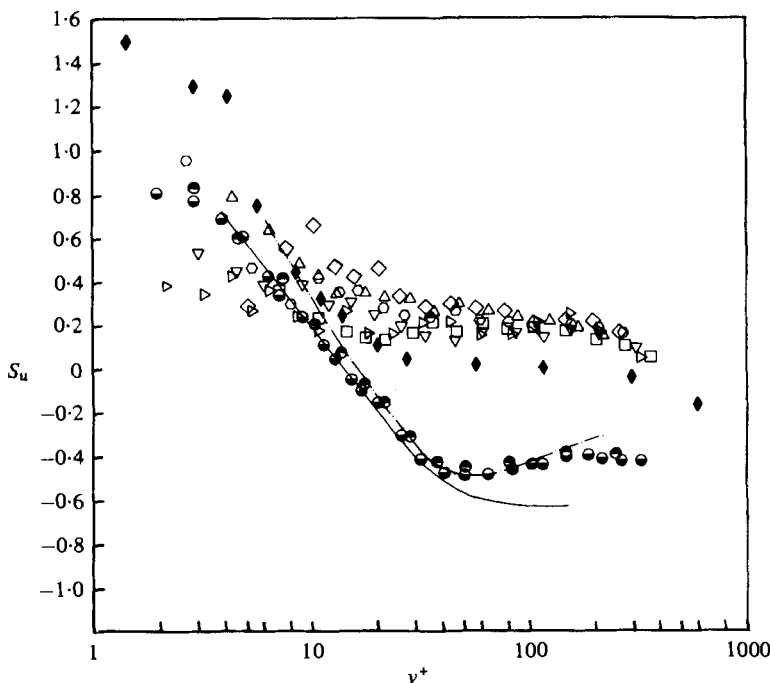


FIGURE 4. Skewness factor, S_u vs. y^+ upstream from detachment: \square , 112.4 in.; \circ , 118.5; \diamond , 120.5; \triangle , 122.6; ∇ , 129.4; \triangleright , 131.9. Ueda & Hinze (1975): \ominus , $Re = 35\,500$; \odot , $Re = 11\,450$. \blacklozenge , Dumas & Marcillat (1966); —, Kreplin (1973); - - -, Zaric (1972).

outer region results in large-amplitude positive u fluctuations and consequently produces a large skirt in the velocity probability distribution. Similarly, near the outer edge of the 'boundary layer, intermittent large-amplitude negative u fluctuations occur as a result of the large eddies driving the fluid from the low velocity regions outwards, which tends to increase the flatness factor. In the buffer layer near a y^+ of 13, the zero pressure gradient flows of Ueda & Hinze, Zaric and Kreplin all show a dip in the F_u flatness factor distributions and a change in sign in the skewness factor S_u distributions for u as shown in figure 4. Ueda & Hinze have remarked that this location is where u' attains the maximum value. The present data show neither any such predominant dip in F_u nor sign change of S_u in the buffer layer. Sandborn's (1959) data for F_u in an adverse-pressure-gradient boundary-layer flow show a behaviour similar to the present data. The present data for F_u and S_u also show reasonable agreement with those of Dumas & Marcillat (1966), but this is anomalous since his zero-pressure-gradient data do not agree with those from other zero-pressure-gradient flows.

The present data for S_u as shown in figure 5(a) indicate a change in sign at a location farther away from the wall ($y/\delta \simeq 0.4$). This location corresponds to the region where the Reynolds shear stress and the turbulent intensities reach their maximum values. The intense momentum exchange in this region results in the lack of occasionally very-high or very-low fluctuations and as a consequence the probability distribution does not have much skewness. As one moves closer to the wall, the intermittent large-amplitude positive u fluctuations tend to make the probability distributions more

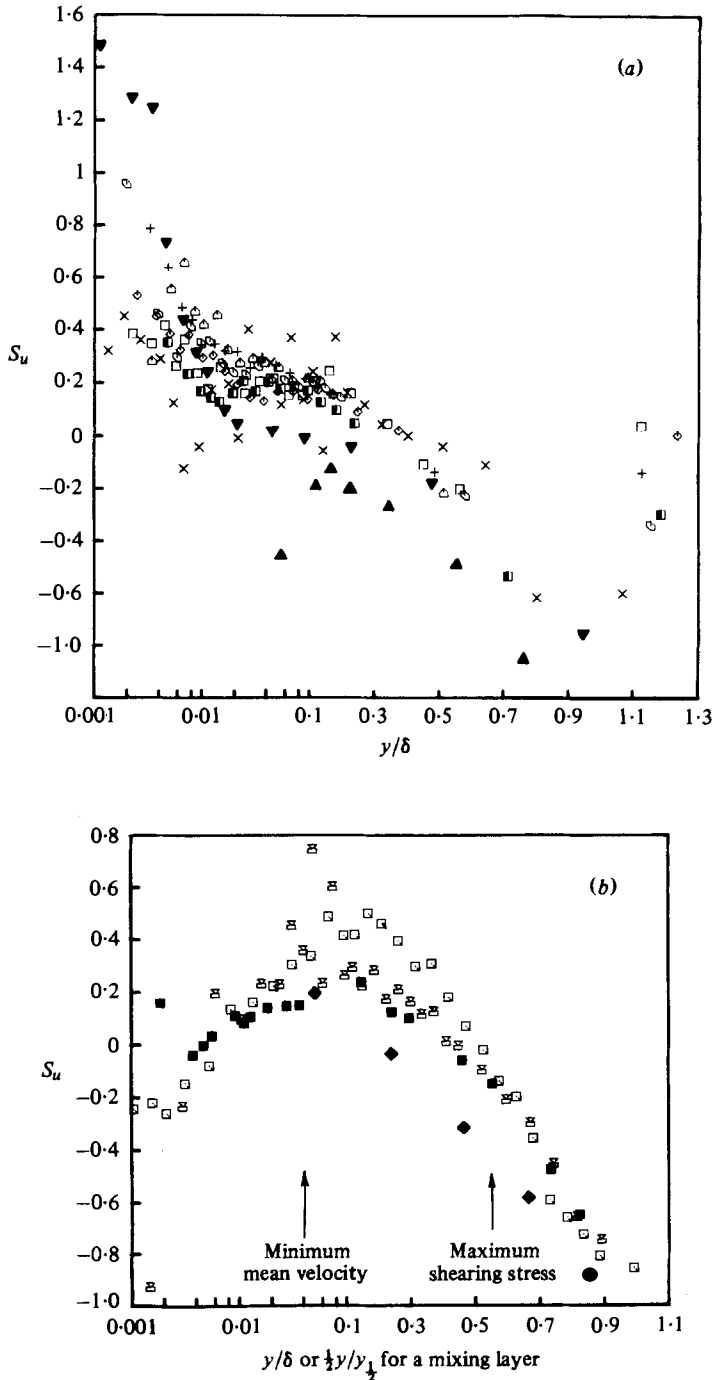


FIGURE 5. Skewness-factor, S_u , laser-anemometer data (a) upstream and (b) downstream from detachment. (a) \blacksquare , 112.4 in.; \square , 118.5; \diamond , 120.5; +, 122.6; \times , 127.1; \diamond , 129.4; \square , 131.9. \blacktriangle , Antonia (1973), $R_\delta = 31000$; \blacktriangledown , Dumas & Marcollat (1966), $R_\delta = 32500$. Note the log-linear abscissa. (b) \blacksquare , 138.75 in.; \boxtimes , 144.9; \square , 156.4. \blacklozenge , Wygnanski & Fiedler (1970), mixing-layer data.

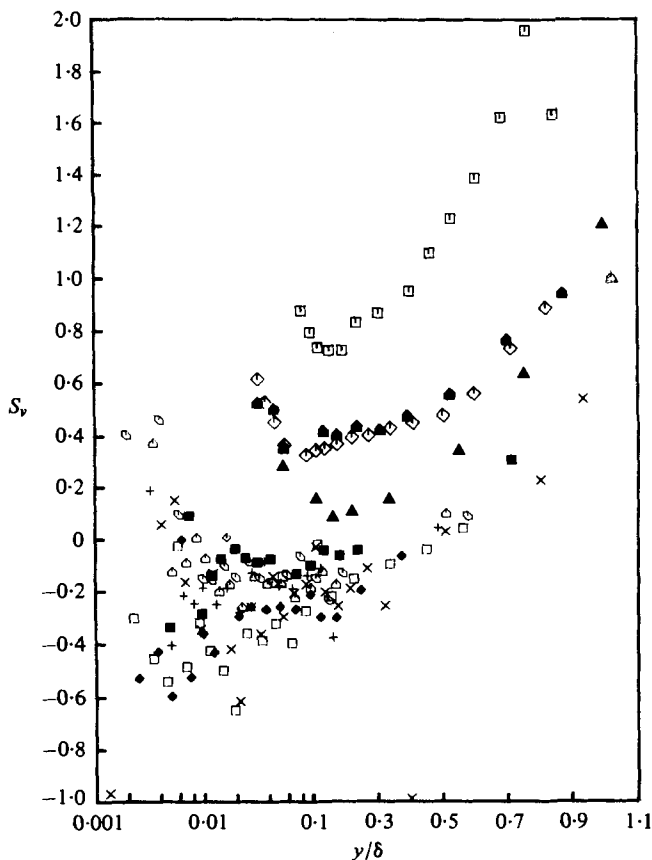


FIGURE 6. Skewness-factor, S_v , data upstream from detachment. Hot-wire data \square , 31.7 in.; \blacktriangle , 86.5; \diamond , 105.25. Laser-anemometer data \blacksquare , 112.4; \square , 118.5; \triangleleft , 120.5; $+$, 122.6; \times , 127.1; \blacklozenge , 129.4; \square , 131.9. \blacktriangle , Antonia (1973), $R_\delta = 31000$. Note the log-linear abscissa.

positively skewed (Eckelmann 1974) and *vice versa* when one moves away from the wall.

The location corresponding to zero skewness for u occurs very close to the wall in zero-pressure-gradient flows because the Reynolds shear stress attains a maximum value in that region. Furthermore, the intense mixing in that region suppresses large-amplitude u fluctuations, thus removing the skirt in the positively skewed velocity probability distribution and changing it to a more nearly top-hat shape with a low flatness factor. The same does not happen in adverse-pressure-gradient flows in the region of maximum shear because the probability distribution in that region is more nearly Gaussian with only a slight skewness and with no significant large-amplitude fluctuations to be suppressed.

Downstream of separation the skewness S_u is reduced to negative values in the backflow region as shown in figure 5(b). A maximum is observed in the vicinity of the minimum mean velocity. As shown in figure 1(b), F_u also has a local maximum near this location. The second zero-skewness point is slightly closer to the wall than the location of the maximum shear stress.

The flatness factor distributions for v in figures 2(a, b) show a trend similar to that

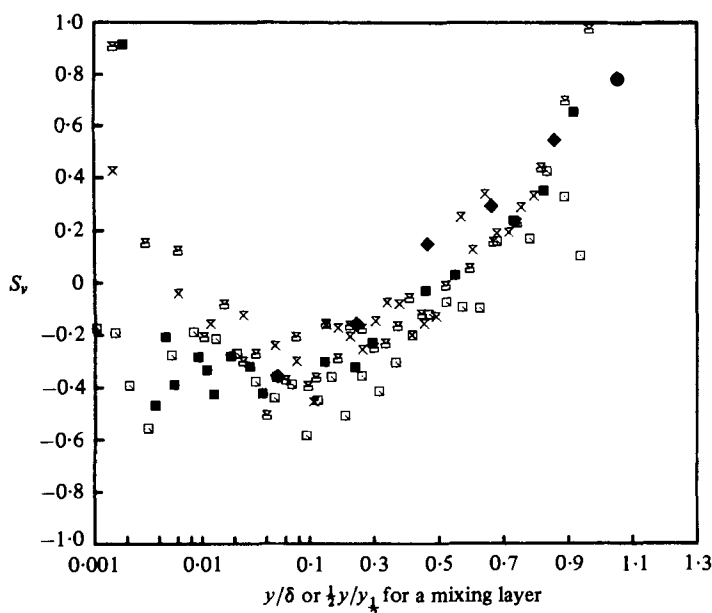


FIGURE 7. Skewness-factor, S_v , data downstream from detachment ■, 138.75 in.; ⋈, 144.9; □, 156.4; ⋈, 170.9. ◆, Wygnanski & Fiedler (1970), mixing-layer data.

of u , the only difference being the reduced width of the flat region. Figures 6 and 7 show that there is a significant variation of S_v along the flow. Only downstream of 132 in. is there profile similarity in the outer region. S_v shown in figure 7 exhibits a shape approximately opposite in sign to that of S_u , with a large positive skewness factor near the outer edge of the boundary layer, gradually decreasing to negative values towards the wall. This results in the appearance of two zero-skewness points in the distributions of S_v both upstream and downstream of separation. The zero-skewness point which is farther from the wall occurs in the region of maximum shear both upstream and downstream of separation, which indicates that the backflow has no influence on the location of this point as in the case of S_u . Downstream of separation the flatness and skewness factors away from the wall are in qualitative agreement with those of Wygnanski & Fiedler (1970) for a plane mixing layer. This is not surprising since the mean-velocity profiles resemble those in mixing layers.

4.2. Diffusion of turbulence kinetic energy

The diffusion term $\partial/\partial y(\overline{pv}/\rho + \frac{1}{2}\overline{q^2v})$ of the turbulence kinetic energy equation is known to become more important as a turbulent boundary layer approaches separation (Bradshaw 1967; Simpson & Collins 1978). The term \overline{pv}/ρ which represents the diffusion flux due to pressure forces cannot be measured directly using available techniques. Normally, it is estimated by the difference of other measurable terms in the turbulence-kinetic-energy equation, although experimental uncertainties make the results quite uncertain. Here the turbulence-kinetic-energy diffusion flux

$$\frac{1}{2}\overline{q^2v} = \frac{1}{2}(\overline{u^2v} + \overline{v^3} + \overline{w^2v}) \quad (2)$$

was estimated using $\overline{u^2v}$ and $\overline{v^3}$ cross-wire anemometer measurements and the approxi-

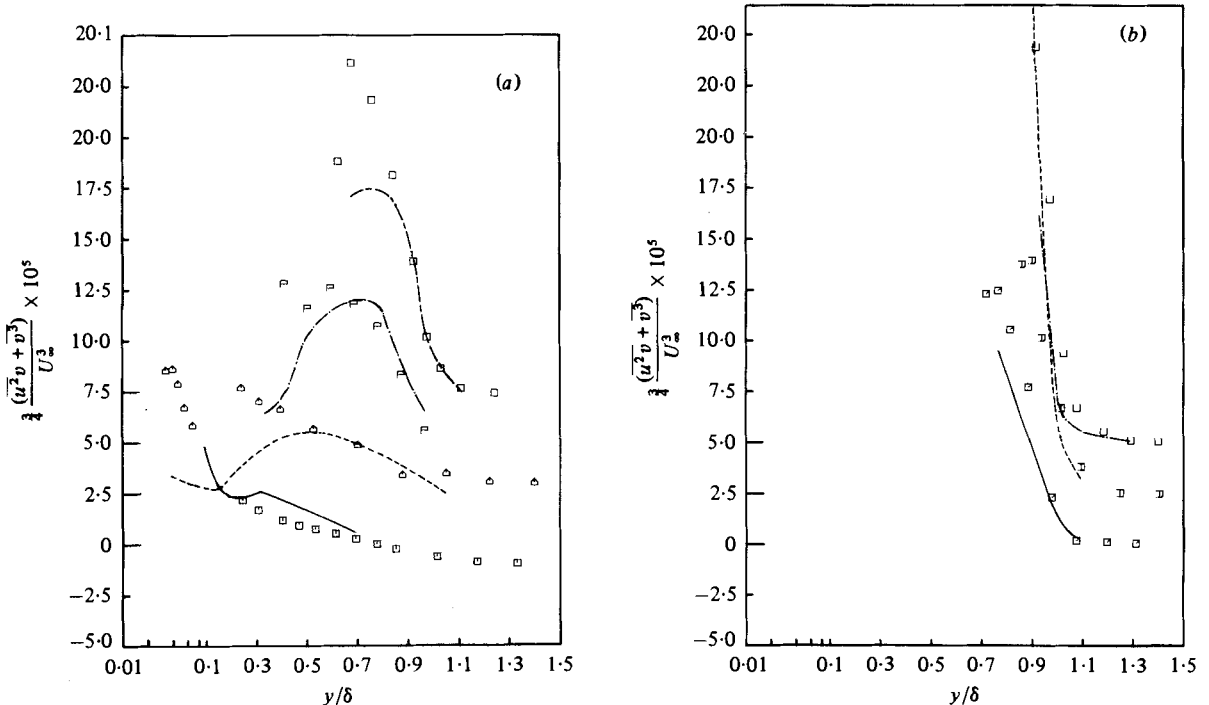


FIGURE 8. Hot-wire results for turbulence-kinetic-energy diffusion flux compared with equation (3) results, which are indicated by lines. (a) \square , —, 31.7 in.; \triangle , ----, 86.5; \square , —, 117.6; \square , ----, 126.8. (b) \square , —, 131.0 in.; \square , ----, 144.0; \square , —, 156.4. Note the displaced ordinates and log-linear abscissa.

mation proposed by Bradshaw (1967), $\overline{w^2v} = \frac{1}{2}(\overline{u^2v} + \overline{v^3})$. (If instead we let $\overline{w^2v} = \overline{v^3}$, since Shiloh, Shivaprasad & Simpson (1981) show that $\overline{w^2} = \overline{v^2}$ in the outer region, and use the approximation that $\overline{u^2v} = 3\overline{v^3}$ from the data of Simpson *et al.* (1980), then the resulting $\frac{1}{3}\overline{q^2v}$ will be $\frac{5}{6}$ of the values shown below using Bradshaw's approximation.

Figure 8(a, b) shows the present results. The flux of turbulence kinetic energy is positive in the regions where data have been plotted, indicating that the flux is directed away from the wall. For locations downstream of 117.6 in. the data are limited only to the region near the outer edge of the boundary layer. Nearer the wall at these locations the flux is expected to be negative, since most of the turbulence-energy production is in the middle of the boundary layer and previous strong adverse pressure gradient data (East & Sawyer 1979) have this behaviour.

East & Sawyer proposed a gradient model based on a mixing length formulation

$$\overline{q^2v} = 0.4l \frac{d}{dy} (\overline{q^2})^{\frac{3}{2}}. \quad (3)$$

They obtained experimental data for seven equilibrium turbulent boundary layers with $U_\infty \sim x^R$ for R approximately equal to 0.4, 0.2, 0, -0.2, -0.4, -0.6 and -0.8. The above model agreed with those data satisfactorily in the outer half of the boundary layer in all cases. Agreement in the inner regions improved for increasingly adverse pressure gradients. Using the mixing length and turbulence-kinetic-energy

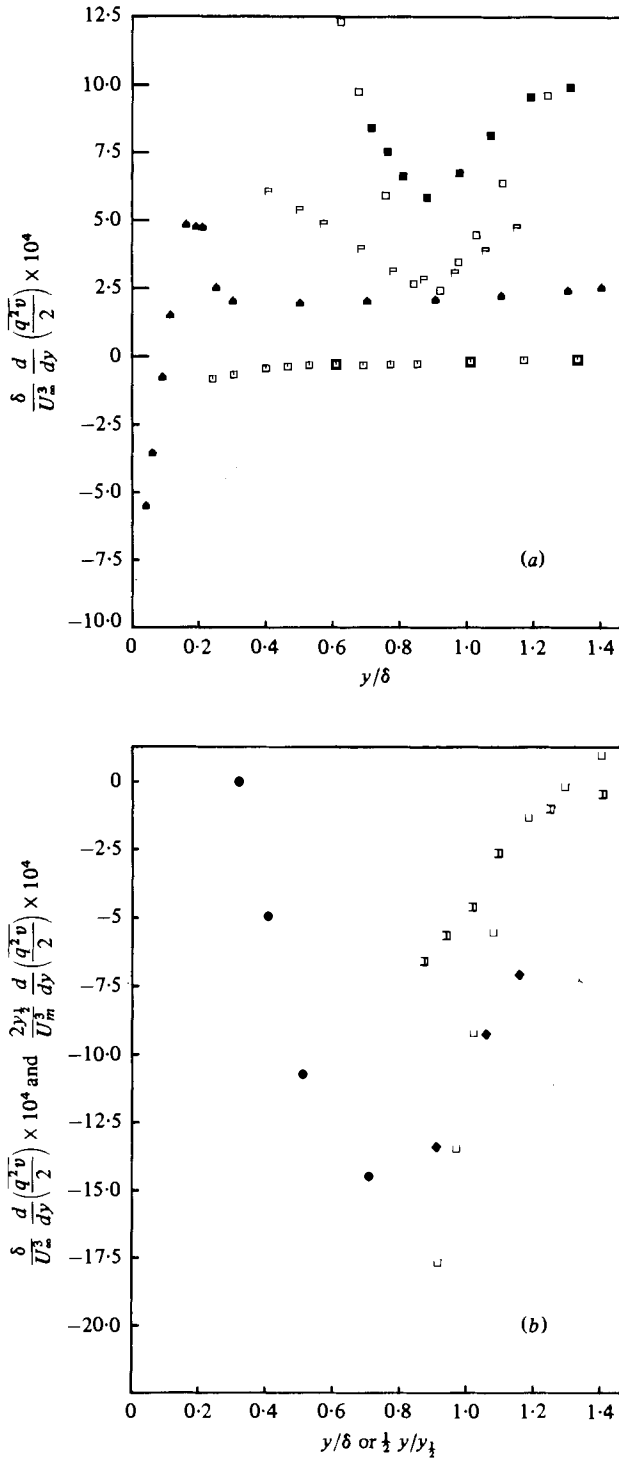


FIGURE 9. Turbulence-kinetic-energy diffusion (a) upstream and (b) downstream from detachment. (a) \square , 31.7 in.; \blacktriangle , 86.5; \square , 117.6; \square , 126.8; \blacksquare , 131.0. Note the displaced ordinates. (b) \square , 144.0 in.; \square , 156.4. \blacklozenge , Wygnanski & Fiedler (1970), mixing-layer data.

distributions obtained from the present non-equilibrium experiments, the results from this model are shown in figure 8(a, b). Agreement in the outer region is within the uncertainty of the measurements. In the inner region only the general shape of the predictions agree with measurements.

It can be observed from figure 9(a, b) that the diffusion is small at the upstream stations and becomes appreciable downstream from 117 in. Farther downstream as separation is approached, the diffusion increases continuously. It is interesting to note that such large negative diffusion rates occur on the low velocity side of mixing layers also. This can be seen in figure 9(b) which has the data of Wygnanski & Fiedler (1970) plotted for comparison with the present data at $x = 156\frac{3}{4}$ in. The maximum velocity in the mixing layer U_m and the total shear-layer thickness $2y_{\frac{1}{2}}$ were used for non-dimensionalizing those data. This similarity in behaviour with the mixing layer suggests that the diffusion, which is responsible for the lateral spread of mixing layers, is also responsible for the rapid growth of separated boundary layers. The large gain of energy by diffusion in the outer region and the associated increase in entrainment of the non-turbulent fluid seems to be responsible for the maintenance of the large eddies and the large growth rates of separated boundary layers.

The entrainment rate of free-stream fluid increases as separation is approached. This can be expressed in terms of the entrainment velocity, V_p , obtained from mean velocity measurements using the relationship

$$V_p = \frac{d}{dx} [U_\infty(\delta_{0.995} - \delta^*)]. \quad (4)$$

Upstream of separation these results are in good agreement with Bradshaw's correlation

$$\frac{V_p}{U_\infty} = 10 \frac{\tau_{\max}}{\rho U_\infty^2} \quad (5)$$

for boundary layer and mixing layers. Downstream of detachment there is poor agreement, in contrast to the good agreement obtained by Simpson *et al.* (1977) for their separating flow.

5. Momentum and turbulence energy balances

In order to understand further the effect of separation on the transport of momentum and turbulence kinetic energy, terms of the governing equations were obtained using the measured quantities described above. The x -direction and y -direction momentum equations are, respectively,

$$U \frac{\partial U}{\partial x} + V \frac{\partial U}{\partial y} = -\frac{1}{\rho} \frac{\partial p}{\partial x} + \frac{\partial(-uv)}{\partial y} - \frac{\partial \overline{u^2}}{\partial x}, \quad (6)$$

$$U \frac{\partial V}{\partial x} + V \frac{\partial V}{\partial y} = -\frac{1}{\rho} \frac{\partial p}{\partial y} + \frac{\partial(-\overline{uv})}{\partial x} - \frac{\partial \overline{v^2}}{\partial y}. \quad (7)$$

For each equation the terms on the left-hand side are inertia or convective terms while the terms on the right-hand side describe the pressure gradient, the shearing-

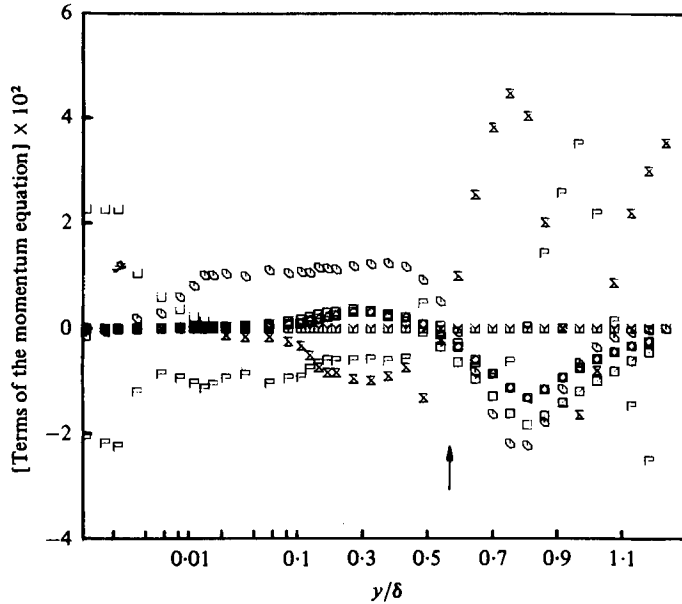


FIGURE 10. x -direction momentum balance at 156.4 in. The arrow denotes the location of maximum shearing stress. Y, $(\delta\nu/U_\infty^2) \partial^2 U/\partial x^2$; P, $-(\delta/U_\infty^2 \rho) \partial P/\partial x$ from equation (6); K, $-(\delta/U_\infty^2) \partial(u'^2 - v'^2)/\partial x$; Q, $(\delta/U_\infty^2) \partial(-\overline{uv})/\partial y$; S, $(\delta/U_\infty^2) U^2 \partial(V/U)/\partial y$; L, $(\delta\nu/U_\infty^2) \partial^2 U/\partial y^2$; M, $-(\delta/U_\infty^2) \partial u'^2/\partial x$.

stress gradient, and the normal-stress gradient, respectively. The turbulence-energy equation is

$$\frac{U}{2} \frac{\partial \overline{q^2}}{\partial x} + \frac{V}{2} \frac{\partial \overline{q^2}}{\partial y} = -\frac{\partial}{\partial y} \left(v \left(\frac{p}{\rho} + \frac{q^2}{2} \right) \right) - \overline{uv} \frac{\partial U}{\partial y} - (\overline{u^2} - \overline{v^2}) \frac{\partial U}{\partial x} + \epsilon. \quad (8)$$

The terms on the left-hand side are advection terms while the terms on the right-hand side describe turbulent diffusion, turbulent-shear-stress production, normal-stresses production, and dissipation, respectively. Dissipation was not measured. In all three equations the viscous terms have been neglected because they are much smaller than the other terms.

An estimate of uncertainties of all the significant terms for a few typical points across the boundary layer are given in table 8 of Simpson *et al.* (1980) for 118.5 in. and 131.875 in. Very near the wall the uncertainties are high, but beyond $y/\delta \simeq 0.02$, the uncertainties of most of the dominant terms are less than 30–40% at many points. In general, the terms involving derivatives with respect to y have less uncertainty compared with those involving derivatives with respect to x , since the latter terms are much smaller and were computed from data acquired on different days. Hence each data point used to determine x derivatives corresponded to slightly different experimental conditions.

An exception to this is the inertia terms of the x -direction momentum equation. In this case the two-dimensional continuity equation can be used to obtain a single term involving only a y derivative of a given velocity profile:

$$U \frac{\partial U}{\partial x} + V \frac{\partial U}{\partial y} = -U^2 \frac{\partial(V/U)}{\partial y}.$$

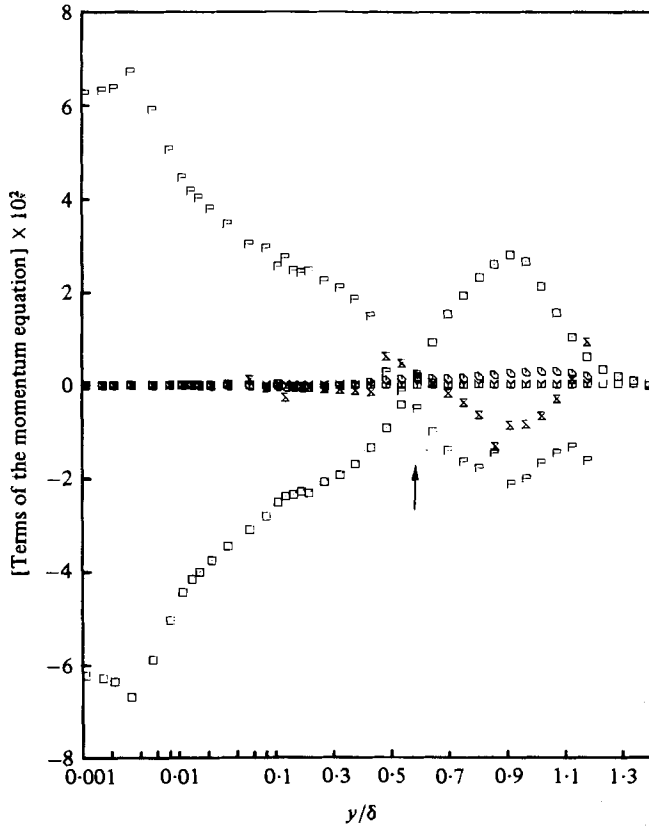


FIGURE 11. y -direction momentum balance at 156.4 in. The arrow denotes the location of maximum shearing stress. Y, $(\delta\nu/U_\infty^2) \partial^2 V/\partial x^2$; P, $-(\delta/U_\infty^2 \rho) \partial P/\partial y$; U, $(\delta/U_\infty^2) \partial(-\bar{uv})/\partial x$; X, $(\delta/U_\infty^2) U^2 \partial(V/U)/\partial x$; V, $(\delta\nu/U_\infty^2) \partial^2 V/\partial y^2$; □, $-(\delta/U_\infty^2) \partial v'^2/\partial y$.

This expression was used only when U was much larger than V , since the uncertainty in V/U becomes large as U approaches zero. The relative uncertainty in this term is large in the outer region because y -direction gradients are small. On the whole, even though the uncertainties are large it is still possible to arrive at certain conclusions regarding the relative importance of the various terms in the momentum and turbulence energy equations as the boundary layer passes through separation.

Although the momentum and energy balances were examined at several stations upstream and downstream of separation by Simpson *et al.* (1980), the results are presented here for one representative station in the fully separated region (156.3 in.). Figures 10 and 11 show the distributions of the various non-dimensional terms of the momentum equations and figure 13 represents the terms of the energy equation. The location of the maximum shear stress $-\bar{uv}$ is shown on all the plots.

Plots given by Simpson *et al.* (1980) and figure 11 indicate that when $\partial(-\bar{uv})/\partial y$ is positive, the only important terms in the y -direction momentum equation are the pressure-gradient and the normal-stress terms. This is true both upstream and downstream of separation and leads to the following simplification of equation (7):

$$-\frac{1}{\rho} \frac{\partial P}{\partial y} = \frac{\partial v'^2}{\partial y}.$$

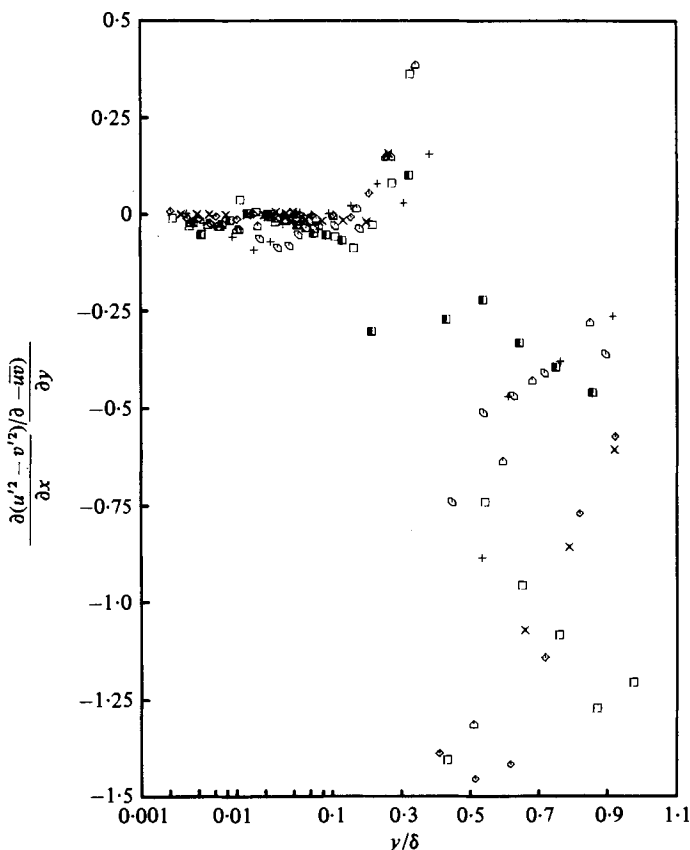


FIGURE 12. Ratio of momentum-equation normal-stresses and shear-stress terms upstream from detachment. \blacksquare , 112.4 in.; \square , 118.5; \triangle , 120.5; +, 122.6; \times , 127.1; \diamond , 129.4; \square , 131.9. Note the log-linear abscissa.

Upon integration it becomes $P(x, y) = P_0 - \rho v'^2$, where P_0 is the wall mean static pressure. Differentiating this equation with respect to x produces

$$\frac{-1}{\rho} \frac{\partial P}{\partial x} = \frac{-1}{\rho} \frac{\partial P_0}{\partial x} + \frac{\partial v'^2}{\partial x}. \quad (9)$$

Since $\partial v'^2/\partial x$ is much smaller than $\partial P_0/\partial x$, the mean pressure gradient is nearly independent of y in the region where $\partial(-\overline{uv})/\partial y$ is positive. Figure 10 also shows the same result where $\partial P/\partial x$ is calculated using equation (6) and measured velocity data. This conclusion applies at all locations upstream and downstream of detachment.

Where $\partial(-\overline{uv})/\partial y$ is negative, the convective term in equation (7) is also important as shown in figure 11 and $\partial P/\partial x$ is not independent of y . Figure 10 shows that this is also the case when $\partial P/\partial x$ is calculated from equation (6).

As shown in figure 10 the convective terms in the x -direction momentum equation are less important in the separated region when $\partial(-\overline{uv})/\partial y$ is positive than in the outer region. Near the wall the momentum transfer due to shear mainly balances the x -direction pressure gradient. In the outer region in addition to the important convective terms, the normal stresses term $\partial(u'^2 - v'^2)/\partial x$ that arises from using equation (9)

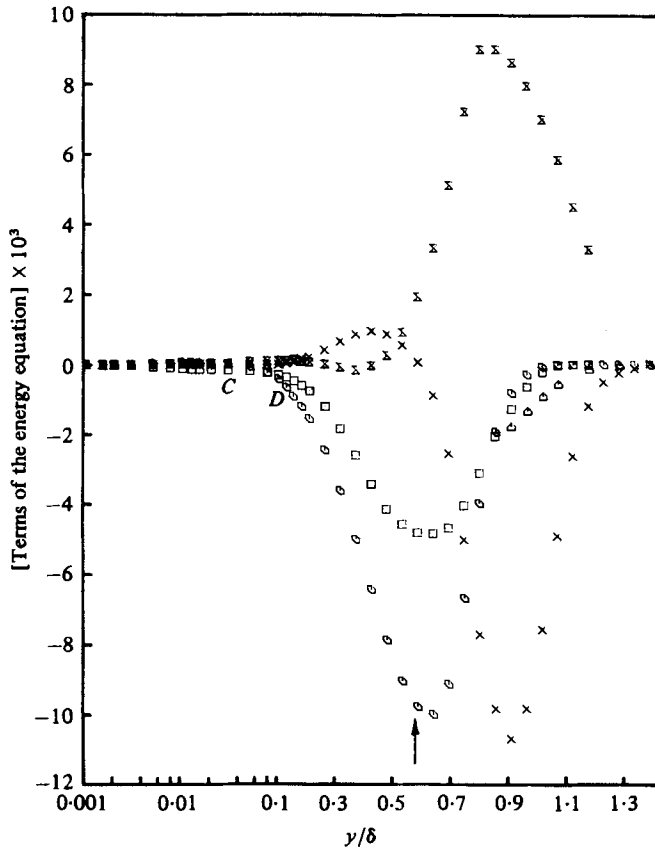


FIGURE 13. Turbulence-energy balance at 156.4 in. with the location of inflection points *C* and *D* described by Shiloh *et al.* (1981). Note the log-linear abscissa. \times , $\frac{1}{2}(\delta/U_\infty^3) U \partial(u'^2 + v'^2)/\partial x$; \times , $\frac{1}{2}(\delta/U_\infty^3) V \partial(u'^2 + v'^2)/\partial y$; \circ , $(\delta/U_\infty^3) \overline{wv} \partial U/\partial y$; \square , $(\delta/U_\infty^3) (u'^2 - v'^2) \partial U/\partial x$; \triangle , $(\delta/U_\infty^3) \partial \frac{1}{2}(u'^2 + v'^2)/\partial y$.

in equation (6) becomes important as separation is approached, as has already been shown by Simpson *et al.* (1977). The normal stresses play an important role in the vicinity of the maximum shear stress. At 118 in., the normal-stresses term is still quite small. The momentum balance at 132 in. shows that the normal-stresses term is more important. Its importance increases progressively downstream as can be seen from figure 10, which shows that this term contributes up to half of the momentum transport in the outer region. This is shown more clearly in figure 12 by the distributions of the ratio of the normal-stresses term to the shear-stress term. However, owing to uncertainties in the gradients the uncertainty of these results in the outer region is large. Thus the inner layer in the separated region could be modelled by neglecting the convective terms while in the outer layer the additional effect of the normal stresses must be included.

Figure 13 and plots presented by Simpson *et al.* (1980) show the importance of the normal stresses turbulence energy production from just upstream of intermittent separation to far downstream as discussed by Simpson *et al.* (1981). The results for the Bradshaw (1967) flow are in qualitative agreement with the data upstream of

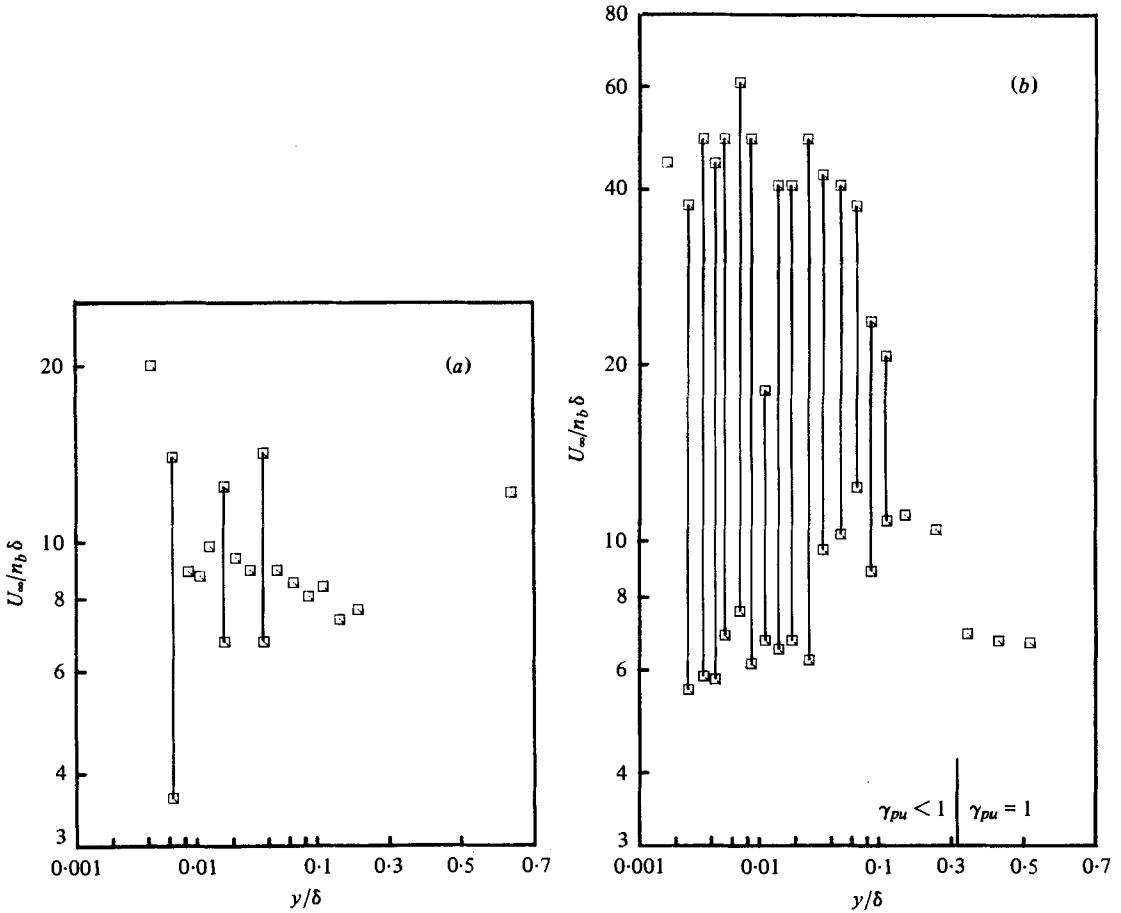


FIGURE 14. Characteristic frequency parameter $U_\infty/n_s \delta$ vs. y/δ at (a) 112.4 in., (b) 134.5 in. and (c) 156.8 in. Note the log-linear abscissa.

separation. As far as shear production alone is concerned, the present data in the region upstream of separation is in agreement with those of Spangenberg, Rowland & Mease (1967) and others who observed two peaks in distributions for boundary layers subjected to large adverse pressure gradients. The present data indicate that as separation is approached, the peak near the wall becomes weaker until it vanishes in the region of fully-developed separation. In the backflow zone of the separated region there is no shear production as indicated by figure 13 and advection is also insignificant. Hence the only mode by which turbulence energy can reach the backflow zone is by turbulent diffusion. This conclusion is consistent with the results discussed in §4.2 above: diffusion plays a major role in transporting the turbulence kinetic energy in separated flows from the middle part of the layer, where it is mainly produced, to the outer region and the region near the wall. The absence of production near the wall in separated flow also leads one to conclude that the backflow near the wall is controlled by the large-scaled outer-region flow, rather than by some wall-shear-stress-related 'law of the wall'.

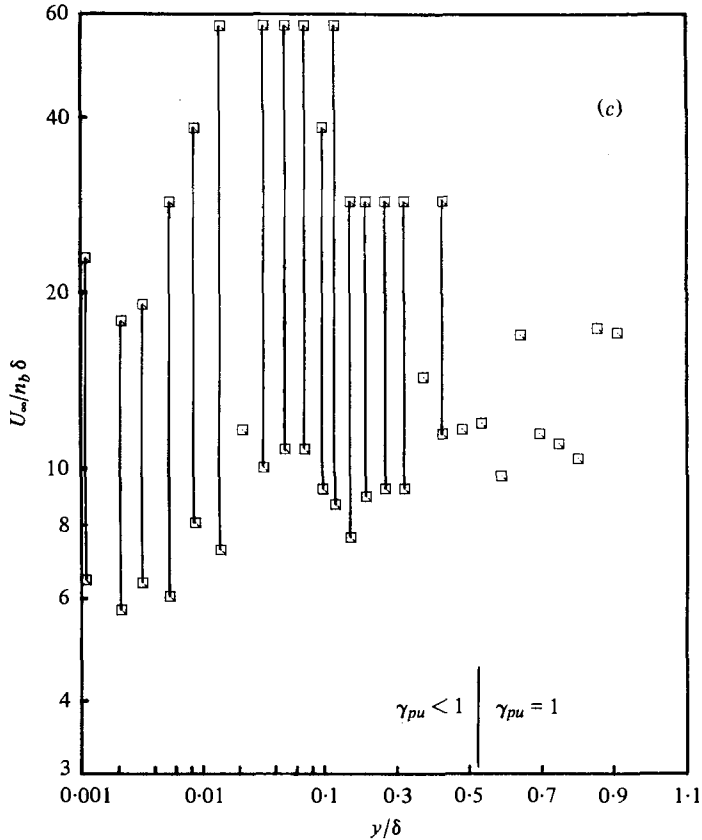


FIGURE 14c. For legend see p. 69.

6. Characteristic frequencies from spectra in separated flow

Strickland & Simpson (1975) showed that the characteristic bursting frequency could be determined by the peak in the first moment of the spectra $nF(n)$ of the wall shearing stress. These characteristic frequencies for the Simpson *et al.* (1977) separating flow correlated with the outer flow velocity and length scales, U_∞ and δ , as do the bursting frequencies for the zero-pressure-gradient case. However, $U_\infty/\delta n_b$ was between 11.7 and 8.35 for that separating flow, whereas values of about 5 are reported for the zero-pressure-gradient case. The basic conclusion of these earlier results is that the characteristic frequency of the most energetic turbulent fluctuations scale on the large-scale structure of the shear flow.

In the earlier work of Simpson *et al.* (1977) no spectral measurements in the separated flow were made. In the present flow spectral data for u were obtained from the laser anemometer velocity signals. Since the LDA signal data rate was under 400 signals/s and signal dropout was present, the spectra are only reliable under 100 Hz. The first moment of each spectral distribution $nF(n)$ was obtained and the frequency of the peak was selected as the characteristic frequency n_b . In many cases the $nF(n)$ peak was constant over a frequency range, which is represented in figure 14 as a line over the range of $U_\infty/\delta n_b$ values for a spectrum at a given y/δ .

Figure 14 shows that upstream of intermittent separation $U_\infty/\delta n_b$ is essentially constant throughout the inner flow region with a value of about 10 ± 3 . At successive downstream locations the range of $U_\infty/\delta n_b$ for a given $nF(n)$ peak becomes progressively larger near the wall as shown in figure 14. In most cases a single frequency characterises the $nF(n)$ peak in the outer region. $U_\infty/\delta n_b$ is about 10 ± 3 at the lower end of the $U_\infty/\delta n_b$ bands. The upper values of $U_\infty/\delta n_b$ are about 40 or so in the inner region.

These results indicate that the characteristic frequency of the outer region correlate with U_∞ and δ along the flow, with an approximately constant value of $U_\infty/\delta n_b$ of about 10 ± 5 . This is consistent with the earlier work of Simpson *et al.* (1977). Nearer the wall the frequency range of the energetic turbulent motions descends to frequencies one-fourth as large.

For attached boundary layers the spectra for the near wall flow have a range of frequencies over which the peak of each $nF(n)$ distribution is constant (Rotta 1962). This is a consequence of the logarithmic law-of-the-wall velocity profile. For a separated flow the law-of-the-wall is not valid, so a different explanation of the $nF(n)$ distribution near the wall is needed. The upper frequency end of the $nF(n)$ peak is at approximately the same frequency as the outer region peak frequency. Note from figure 14 that the wide frequency spectral plateaux seem to occur at locations near the wall where $\gamma_u < 1$.

One simple speculation is that the celerity or speed of the eddies in the backflow region is much lower than that in the outer region. Simpson *et al.* (1977) show that the wall speed of the eddies associated with the characteristic frequency decreases to a small fraction (about $\frac{1}{4}$) of the outer region celerity as separation is approached. Thus, as large scale structures pass through the outer flow at a frequency of about $U_\infty/10\delta$, these same structures move at a much lower celerity in the backflow region, producing a much lower frequency spectrum.

7. Conclusions on the nature of separating turbulent boundary layer

New information about the structure of a separating turbulent boundary layer has been presented for the separating turbulent boundary layer described in part by Simpson *et al.* (1981). Previous conclusions are also confirmed by these results.

The spectral results confirm the conclusion of Simpson *et al.* (1977) that the frequency of passage of the outer region large scale eddies n_b scales on the free-stream velocity U_∞ and the boundary-layer thickness δ . A new result is that while $U_\infty/\delta n_b$ is about 10 ± 3 in the outer region of the separated flow, a characteristic frequency range exists in the backflow with $10 \pm 3 < U_\infty/\delta n_b < 50 \pm 10$.

Upstream of separation the skewness S_u and flatness F_u factors behave in a similar manner to those of previous adverse-pressure-gradient investigations. In the separated flow between the wall and the locations of the minimum mean velocity, the skewness factor for u , S_u , is negative. Between this point and the location of the maximum shearing stress, S_u is positive. Farther from the wall S_u is negative again. The flatness factor F_u reaches a local maximum of about 4 at the minimum mean velocity location. S_v has a profile shape and magnitudes that are approximately the mirror image or negative of S_u .

As pointed out by Simpson *et al.* (1977), normal-stresses effects contribute signifi-

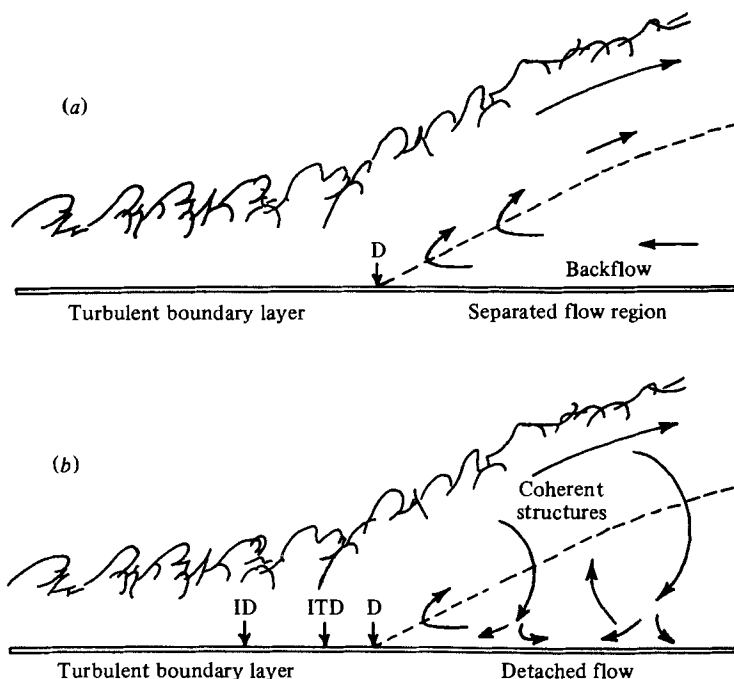


FIGURE 15. (a) Traditional view of turbulent-boundary-layer separation with the mean backflow coming from far downstream. The dashed line indicates $U = 0$ locations. (b) A flow model with the coherent structures supplying the small mean backflow. ID denotes *incipient detachment*; ITD denotes *intermittent transitory detachment*; D denotes *detachment*. The dashed line denotes $U = 0$ locations. See figure 8 of Simpson *et al.* (1981).

cantly to the momentum and turbulence-energy equations. Negligible turbulence energy production occurs in the backflow. Normal-stresses and shear-stresses production in the outer region supply turbulence energy to the backflow by turbulent diffusion. These results are consistent with the absence of a logarithmic mean velocity profile in the backflow, since classical turbulence energy production arguments indicate that the rate of production must equal the rate of dissipation in such a region.

These turbulence-energy results lead to the conclusion that the backflow is controlled by the large-scale outer region flow. Movies of laser-illuminated smoke also have clearly revealed that the large eddy structure supplies most of near wall backflow. The small mean backflow does not come from far downstream as suggested in figure 15(a), but appears to be supplied intermittently by large-scale structures as they pass through the separated flow as suggested by figure 15(b). Thus, as pointed out by Simpson *et al.* (1981), the Reynolds shearing stresses in this region must be modelled by relating them to the turbulence structure and not to local mean velocity gradients. The mean velocity profiles in the backflow are a result of time-averaging the large turbulent fluctuations and are not related to the cause of the turbulence.

A simple qualitative experiment was performed to determine qualitatively the influence of the downstream near wall conditions on the separation behaviour. A deflection plate was located at the end of the second section of the wind tunnel (200 in.) as shown at position *A* in figure 1 of Simpson *et al.* (1981). For heights of this deflection plate up to 7 in., no appreciable change in the separation zone location (122–140 in.)

and behaviour were noted. This result also seems to support the flow model suggested in figure 15(b) where the backflow is supplied locally by outer region large-scale structures. Only after the deflection plate was high enough to begin to change the free-stream pressure gradient did the location of the separation zone change.

Of course, this mechanism for supplying the backflow may be dominant only when the thickness of the backflow region is small compared with the turbulent shear-layer thickness, as in the present case. Experiments (Fox & Kline 1962) on separation in wide-angle diffusers indicate that the mean backflow can come from far downstream when the thickness of the backflow region is comparable to the thickness of the forward flow.

This work was supported by Project SQUID, an Office of Naval Research Program.

REFERENCES

- ANTONIA, R. A. 1973 *Phys. Fluids* **16**, 1198–1206.
 BRADSHAW, P. 1967 *J. Fluid Mech.* **29**, 625–645.
 DUMAS, R. & MARCILLAT, J. 1966 *C. R. Acad. Sci. Paris A* **262**, 700–703.
 EAST, L. F. & SAWYER, W. G. 1979 *Proc. NATO-AGARD Fluid Dynamics Symp.*
 ECKELMANN, H. 1974 *J. Fluid Mech.* **65**, 439–459.
 FOX, R. W. & KLINE, S. J. 1962 *Trans. A.S.M.E. D, J. Basic Engng.* **84**, 303–312.
 KREPLIN, H.-P. 1973 M.Sc. thesis, Max-Planck-Institut für Strömungsforschung, Göttingen.
 PERRY, A. E. & SCHOFIELD, W. H. 1973 *Phys. Fluids* **16**, 2068–2074.
 ROTTA, J. C. 1962 *Prog. Aeron. Sci.* **2**, 1–219.
 SANDBORN, V. A. 1959 *J. Fluid Mech.* **6**, 221–240.
 SHILOH, K., SHIVAPRASAD, B. G. & SIMPSON, R. L. 1981 *J. Fluid Mech.* **113**, 75–90.
 SIMPSON, R. L. & CHEW, Y.-T. 1979 *Proc. of 3rd Int. Workshop on Laser Velocimetry*, pp. 179–196. Hemisphere.
 SIMPSON, R. L., CHEW, Y.-T. & SHIVAPRASAD, B. G. 1980 Project SQUID Rep. SMU-4-PU. (To appear as DTIC or NTIS Report.)
 SIMPSON, R. L., CHEW, Y.-T. & SHIVAPRASAD, B. G. 1981 *J. Fluid Mech.* **113**, 23–51.
 SIMPSON, R. L. & COLLINS, M. A. 1978 *A.I.A.A. J.* **16**, 289–290.
 SIMPSON, R. L., STRICKLAND, J. H. & BARR, P. W. 1977 *J. Fluid Mech.* **79**, 553–594.
 SPANGENBERG, W. G., ROWLAND, W. R. & MEASE, N. E. 1967 *Fluid Mechanics of Internal Flow* (ed. G. Sovran), pp. 110–151. Elsevier.
 STRICKLAND, J. H. & SIMPSON, R. L. 1975 *Phys. Fluids* **18**, 306–308.
 UEDA, H. & HINZE, J. O. 1975 *J. Fluid Mech.* **67**, 125–143.
 WYGNANSKI, I. & FIEDLER, H. E. 1970 *J. Fluid Mech.* **41**, 327–361.
 ZARIC, Z. 1972 *4th All-Union Heat and Mass Transfer Conf. Minsk, U.S.S.R.*